Journal of Computational Electronics 4: 221–230, 2005

An Inductive Link with Integrated Receiving Coil—Coupling Coefficient and Link Efficiency

JIE WU
Department of Electrical and Computer Engineering, University of Tennessee, Knoxville, TN 37996

VICTOR QUINN
Tabtronics Inc., Piffard, NY 14454

GARY H. BERNSTEIN
Department of Electrical Engineering, University of Notre Dame, Notre Dame, IN 46556

Abstract. Inductive powering can free microelectromechanical systems (MEMS) devices from tethering to a power supply, thus expanding their scope of applications. We investigate inductive powering for MEMS using a microfabricated coil as a receiver operating at and below 1 MHz. The microcoil is designed to enclose the MEMS functions to achieve maximum coupling, and is built into a silicon substrate by our inlaid electroplating process, so that the microcoil has a small resistance despite its long trace. Non-negligible parasitic effects from the silicon substrate affect the characterization of an inductive link and its optimization. Taking into account the parasitic effects of Si microcoils, the coupling coefficient of the link is determined by a coil-model scheme that is different from conventional strategies. Furthermore, an equivalent circuit is developed for our link and used to analyze link operation over the frequency range of 4 kHz to 4 MHz. With measured link parameters, link efficiency is calculated with our equivalent circuit, and the results agree better with experiments than do conventional models. The equivalent circuit also indicates that microcoils with high quality factor at low frequencies, such as our inlaid electroplated coils, improve link performance, while parasitic capacitance has little effect.

Keywords: MEMS, inductive coupling, deep brain stimulation, inductive link

1. Introduction

The field of microelectromechanical systems (MEMS) promises a new revolution in miniaturized functionality. However, many MEMS devices require either power or voltage that are not consistent with miniaturized, portable sources. In some important cases, such as implantable medical devices, it is feasible to envision inductively powered MEMS where the driving coil can be placed in proximity close enough to the implanted system to be of use. In this paper we present a study of the properties of an inductive link with a microfabricated, on-chip coil that is compatible with standard CMOS processing. This paper addresses overall inductive link performance in terms of the interplay between the driving coil and the integrated receiving microcoil.

Extensive research has been performed to analyze and optimize the operation of inductive links [1–8], and there exist many applications of inductive links to deliver power and data into implanted devices [9, 10]. Recently, microfabricated coils have been adopted as receivers in inductive links to reduce the size of the receiving side and to explore the possibility of integration with other micro-devices to establish a system-on-a-chip [11–15]. It is highly desirable to exploit the miniaturization made available by planar processing, and to determine the link properties of integrated receiving coils.

Due to the planar fabrication process, integrated coils suffer from parasitic effects such as series resistance along metal traces, capacitive coupling between lines, and eddy currents induced in conductive silicon substrates, which may affect the performance of inductive links. Integrated coils for inductive powering have been successfully demonstrated [11–17]. However, in these reports, no details of the driving coils or analysis of the inductive link, such as coupling coefficient and efficiency, were provided.

Here we report a prototype inductive link with an integrated receiving coil for a disposable lab-on-a-chip. Inductive coupling requires no direct electrical connections, reduces the cost of chip packaging and simplifies chip handling. Because the power transfer efficiency of an inductive link can be improved by increasing the area enclosed by its receiving coil, and a microfluidic system can reasonably cover an area of many square millimeters, the microcoil is designed to encircle the lab-chip. For our case, the microcoil is a 10-turn square spiral with a 14 mm maximum side length.

Two salient features of our inductive link are the "inlaid electroplated" copper coil (the fabrication process is reported elsewhere [18, 19]) and its low frequency of operation. Microcoils electroplated in the silicon wafer possess low internal resistance despite their long trace length, but may suffer from greater capacitive coupling through the Si substrate.

To better take into consideration the parasitic effects from microcoil fabrication and silicon substrates, we have modified techniques from conventional ones to characterize and simulate the inductive link. Calculations from our models provide more accurate predictions of link performance. It is found in this study that for the frequency range of interest, microcoil capacitance has little impact on link efficiency, while a high quality factor (Q) will be critical. Inlaid microcoils are favorable for this application because their Q's (of $\sim$20) peak around 1 MHz. Our work intends to provide insights into inductive powering with integrated coils, and it should be noted that the analytical methods and the results of this study lend themselves well to implantable applications.

2. An Inductive Link with Integrated Receiving Coil

The inductive link studied here is composed of a wire-wound driving coil around a ferrite core, and an integrated coil on a silicon wafer as the receiver. The core

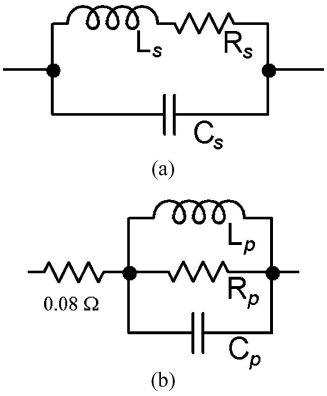

Figure 1. (a) Series coil model, and (b) Parallel coil model.

is made from Philips 3F3 [20] with a cross-sectional area of 8×8 mm^2 and an outer dimension of 50×40 mm^2. It consists of two pieces with an air gap fixed at 2 mm, where the integrated receiving coil is inserted.

Integrated coils are known to exhibit non-negligible parasitic effects because of small dimensions imposed by planar processing techniques. There exists relatively large series resistance caused by the small metal thickness, and parasitic capacitance shunting the inductor due to both the close proximity of the metal lines and electric fields through the oxide to the substrate. The parasitic effects are distributed, but to simplify analysis, a lumped-element model is used, as shown in Fig. 1(a). Because the substrate is floating, one capacitor is used to account for both the interwinding capacitance and that between the copper and the substrate.

The driving coil is a wire-wound solenoid, and so exhibits small DC series resistance. However, since a ferrite core is used to provide positive magnetization, energy is consumed. In addition, since the receiving coil is built on a conductive silicon substrate, eddy currents are induced in the chip when it is inserted in the gap, which gives rise to additional energy dissipation. Both effects can be simulated by placing a resistor in parallel with the coil inductance to account for energy losses. The model is shown in Fig. 1(b). The capacitor represents coupling between coil loops.

Imperfect coupling is inherent to inductive links with separated coils. The degree of coupling between two coils is defined by the coupling coefficient, k. The relationship between the voltage V_1 and current I_1 on the driving side is,

$$V_1 = j\omega(1-k^2)L_1 I_1 + \left(\frac{j\omega k^2 L_1 \cdot k^2 \frac{L_1}{L_2} Z_L}{j\omega k^2 L_1 + k^2 \frac{L_1}{L_2} Z_L}\right) I_1, \tag{1}$$

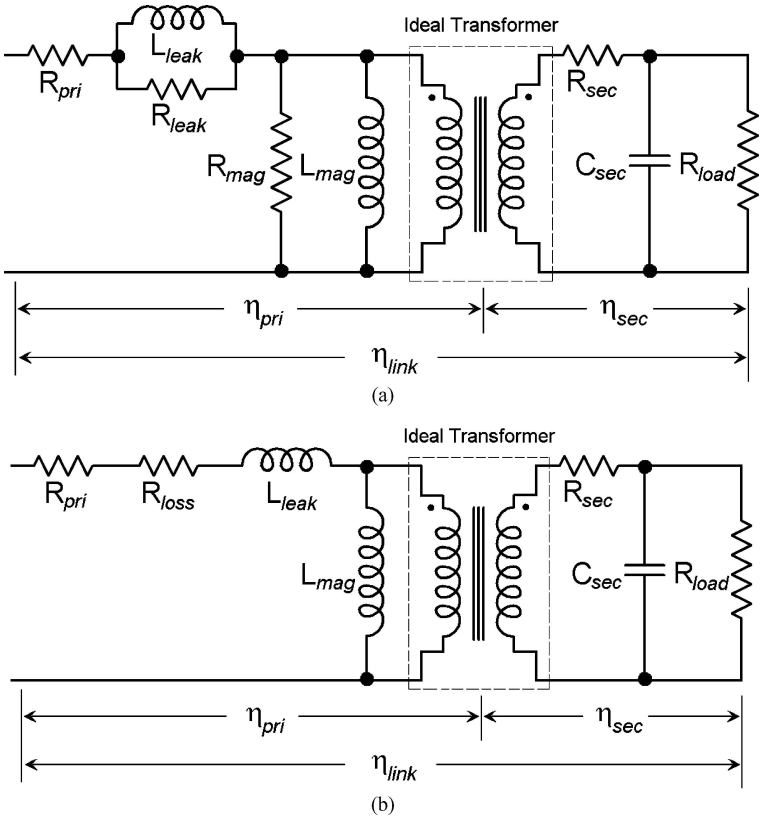

Figure 2. (a) Equivalent circuit for inductive link in this work and (b) commonly used equivalent circuit.

where L_1 and L_2 are the driving coil and receiving coil inductances, respectively, and Z_L is the load impedance. The first term on the right side accounts for magnetic flux leakage in the magnetic path, where $(1-k^2)L_1$ is the leakage inductance, L_{leak}. The load impedance on the receiving side is reflected onto the driving coil multiplied by a factor of $k^2\frac{L_1}{L_2}$, and is in parallel with the magnetizing inductance, $L_{\text{mag}} = k^2 L_1$.

Combining the coil models and the transformation of link coupling (Eq. (1)), an equivalent circuit of our inductive link is developed, as shown in Fig. 2(a). The driving coil inductance, L_1, is separated into leakage inductance, L_{leak}, accounting for imperfect coupling, and magnetizing inductance, L_{mag} ($L_1 = L_{\text{mag}} + L_{\text{leak}}$). In this model, the loss resistor of the driving coil is also separated into R_{mag} and R_{leak}: $R_{\text{mag}} = k^2 R_1$ and $R_{\text{leak}} = (1-k^2)R_1$. This division does not affect the equivalent turns ratio of the inductive link. R_{PRI} is the driving coil DC resistance (less than 0.08 Ω), and can be neglected in the analysis. The accuracy of this treatment will be evaluated in subsequent comparisons of measured results to analytical predictions.

In comparison, the conventional equivalent circuit, as illustrated in Fig. 2(b), assigns the loss resistor totally to the leakage inductance. This practice could be valid for inductive links with both wire-wound coils, where the loss resistor is less significant. In our case, integrated coils cause energy loss to the driving coil from eddy currents in the substrate, so the loss mechanism is distributed, and therefore the loss resistor calls for more careful treatment here.

Only the voltage impressed across the magnetizing inductance is transferred to the receiving coil side by an ideal transformer (a theoretical construct) of equivalent turns ratio: $\frac{N_2}{N_1} = \frac{1}{k}\sqrt{\frac{L_2}{L_1}}$. On the receiver side, R_{sec} and C_{sec} are the internal resistance and parasitic capacitance of the integrated coil, respectively. They are treated as loads, whose impedances are reflected to the driving coil side scaled by the square of the turns ratio.

The power transfer efficiency of an inductive link, η_{link}, is defined as the ratio of power reaching the load to that input to the driving coil. Using our model, the

link efficiency is obtained as:

$$\eta_{\text{link}} = \frac{k^2(Q_1 + 1/Q_1)\cdot 1/a}{k^2(1/Q_2 + 1/a)(Q_1 + 1/Q_1 + 1/Q_2 + 1/a) + (1-k^2)[1 + (1/Q_1 + 1/Q_2 + 1/a)^2]}. \quad (2)$$

Our model differs from the other models for inductive links with two wire-wound coils (refs. [1–6]) in that those models adopt the series (as opposed to our parallel) model (Fig. 1(b)) for the wire-wound driving coils, which leads to an equivalent circuit as shown in Fig. 2(b). An expression for link efficiency is given by Van Schuylenbergh as Eq. (3):

$$\eta'_{\text{link}} = \frac{1}{1 + \frac{a}{Q_2} + \frac{a}{k^2 Q_1} + \frac{1}{k^2 a Q_2} + \frac{2}{k^2 Q_1 Q_2} + \frac{a}{k^2 Q_1^2 Q_2}}. \quad (3)$$

In Eqs. (2) and (3), Q_1 and Q_2 are the quality factors of the driving and receiving coils, respectively, and a is defined as $a = \omega L_2/R_L$. The parallel capacitance of the integrated coil is neglected in the analysis, which is justified in Section 4.

In these conventional models, the loss resistor is placed in series with the effective inductive link, which is valid if the energy losses of the link arise mainly from the DC resistances of the coils. However, with our inductive link, it can be experimentally demonstrated that the conductive silicon substrate introduces additional energy losses for the link. Consequently, the underlying assumptions for link equivalent circuits need to be examined carefully. The validity of our model and that of Van Schuylenbergh will be examined in a later section using experimentally obtained Q values.

3. Inductive Link Characterization

Here we discuss the extraction of element values in coil models and determine the link coupling coefficient from coil impedance measurements. Measuring the impedance amplitude (Z) and phase angle, or real (R) and imaginary (X) components, allows the extraction of equivalent component values, L, C and R of our input and output coils. These are later used to obtain coupling coefficients and link efficiencies—two important parameters for describing the quality of both the wire-wound and integrated coils and their utility in inductive links for such applications as implanted devices.

3.1. Receiving Coil Characterization

The microcoil is a 10-turn square spiral with a 14 mm maximum side length, and the copper lines are 80 μm wide on a 100 μm pitch. The microcoil is fabricated using a special "inlaid electroplating" process developed by us [18, 19]. The silicon wafers are ~575-μm-thick, 4-inch single-crystal silicon ⟨100⟩ wafers, doped n-type with resistivity 5–10 Ω·cm. There is no electrical connection between the coil and substrate, so the substrate is left floating.

Wire-wound coils can have Q's ($Q = \omega L_s/R_s$) of several hundred, but integrated coils, typically RF inductors, have Q's of no more than 10 due to their small dimensions and limited turn numbers. Our metal thickness is increased from the typical ~1 μm by standard IC technology to 54 μm by our inlaid electroplating, increasing Q, as discussed below. A scanning electron micrograph of an inlaid coil after partially removing the silicon substrate is shown in Fig. 3(a). (Since silicon is used as the molding material in this process, the electroplated metal structures can achieve thickness comparable to that from the LIGA process and obviate ionizing-radiation and planarization issues associated with the latter [21], thus preserving the potential of coil integration with electronics.)

The receiving coil impedance was measured using an Agilent 4294A impedance analyzer over the frequency range from 40 Hz to 110 MHz. The model shown in Fig. 1(a) was used to extract lumped elements. A comparison of measured coil impedance with calculated values from the model is given in Fig. 3(b). When the receiving coil is inserted into the air gap, the model elements are extracted as $L_S = 7.4$ μH, $R_S = 2.25$ Ω, and $C_S = 128.6$ pF. Its quality factor is shown in Fig. 3(d). Our inlaid coils have a Q of about 20 around 1 MHz, which is large for integrated coils because our coils are for power delivery and of large dimensions, leading to a large inductance (μH range compared with nH for RF coils). Parasitic effects associated with large size (e.g. parasitic capacitance and energy dissipation in Si substrate) play a minor role over the operating frequency range of our inductive link (<6 MHz).

3.2. *Driving Coil Characterization*

To illustrate the energy dissipative effects of the silicon substrate, the impedance of a 20-turn split driving coil is plotted from 40 Hz to 110 MHz in Fig. 3(c) with and without a silicon chip in the air gap. A bare silicon wafer was used instead of one with integrated coil to avoid the complexity from reflected impedances of the integrated coil. By curve-fitting, the components in the model are determined as: $L_{\mathrm{p}} = 29.0\ \mu\mathrm{H}$, $R_{\mathrm{p}} = 2.25\ \mathrm{k}\Omega$, $C_p = 19.6$ pF without the wafer in the gap, and $L_{\mathrm{p}} = 13.2\ \mu\mathrm{H}$, $R_{\mathrm{p}} = 1.20\ \mathrm{k}\Omega$, $C_{\mathrm{p}} = 19.6$ pF with the wafer in the gap. R_{p} represents core losses when the wafer is not in the gap; when the wafer is in the gap, the energy loss by eddy currents is also included. It is also noted that the driving coil inductance decreases as

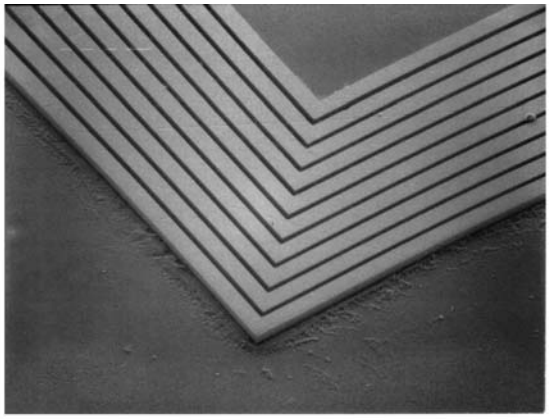

(a)

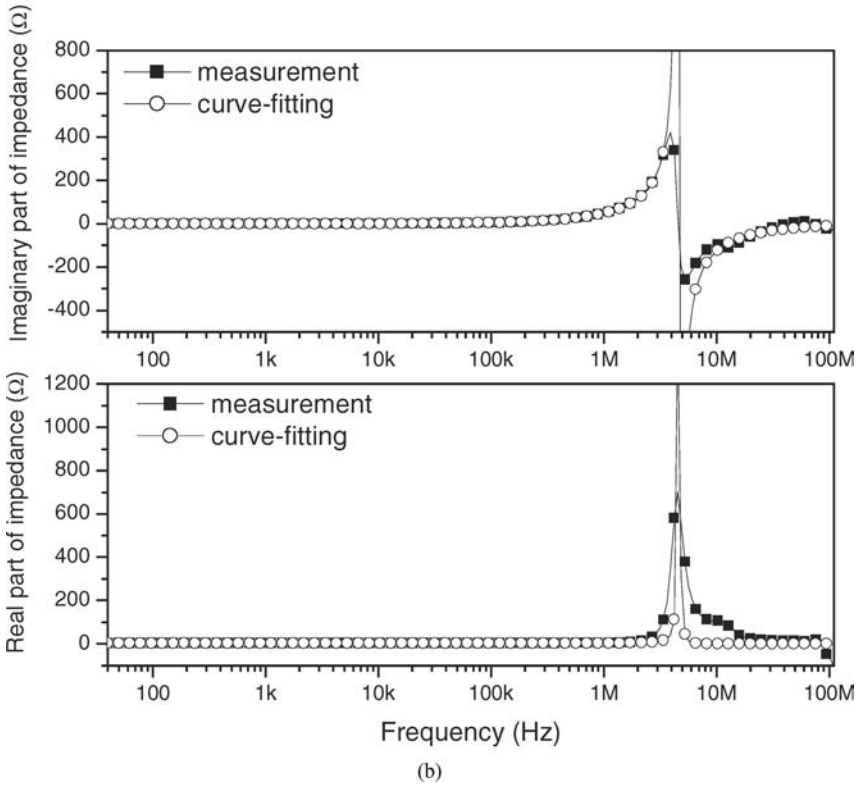

(b)

Figure 3. (a) Optical micrograph of integrated coil, (b) impedance measurement and curve-fitting of integrated coil, (c) impedance measurement and curve-fitting of 20-turn split driving coil, and (d) quality factors of driving and receiving coils. (*Continue on next page*.)

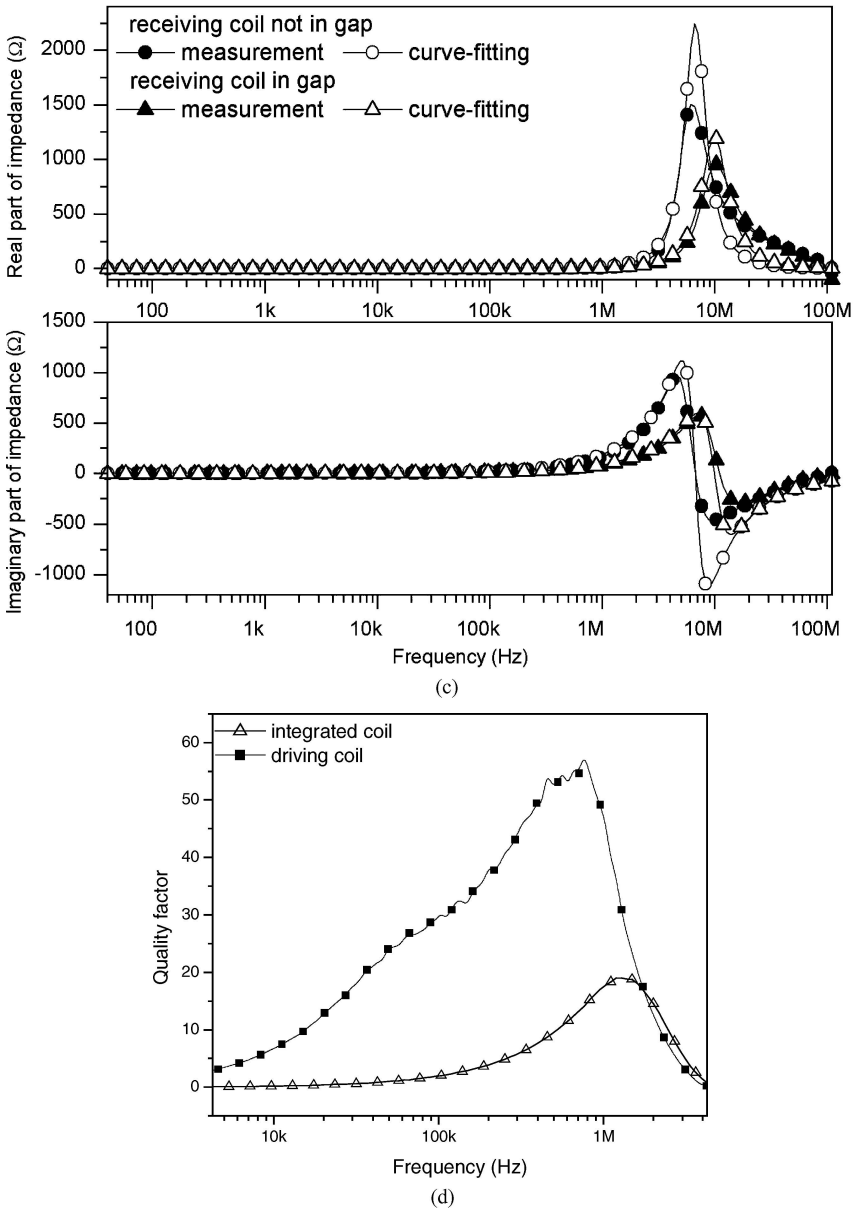

Figure 3. (*Continued.*)

expected when the wafer is in the gap due to reduced flux fringing resulting in a larger equivalent reluctance. Its quality factor, defined as $Q = R_P/\omega L_P$ for the model in Fig. 1(b), is plotted in Fig. 3(d) along with that of the integrated coil.

3.3. Coupling Coefficient

From Eq. (1), with $Z_L = 0$, i.e. short-circuited receiving coil, the inductance looking into the driving coil is $L_{leak} = (1 - k^2)L_1$. With known driving coil inductance, k can be found. Typically, one measures the inductance of one coil with the other one first open-circuited (L_1) then short-circuited (L_{leak}), and $k = \sqrt{(L_1 - L_{leak})/L_1}$. Theoretically, the obtained k should be identical for measurements performed on either side of inductive links, but as we demonstrate below, non-negligible parasitics may lead to different results for measurements from different sides. This is because the $Z_L = 0$ condition cannot be satisfied if the

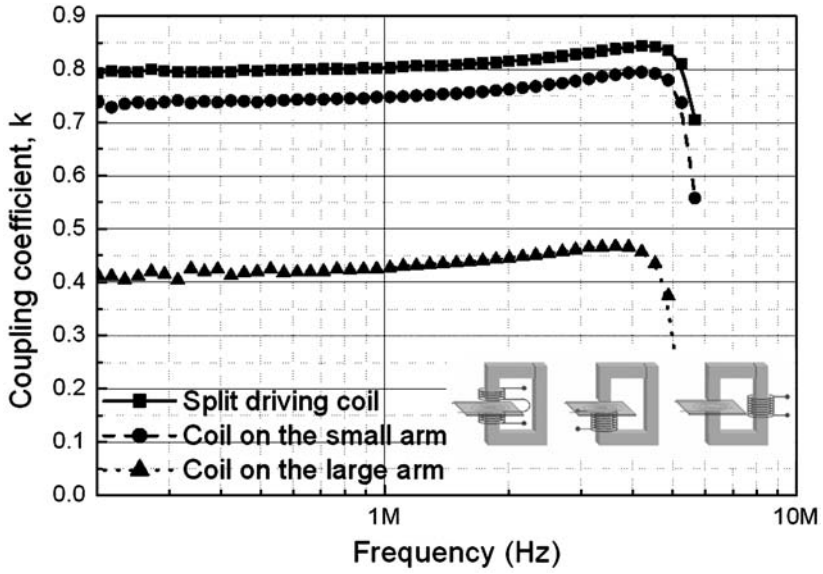

Figure 4. Measured coupling coefficients for three driving coil placements.

measurement is carried out from the wire-wound coil side due to non-negligible parasitics of the integrated receiving coil, which are regarded as the equivalent load. Alternatively, the measurement can be performed from the integrated coil side. Figure 4 shows k for the three inductive link configurations shown in the inset. From left to right, they are labeled as the coil on the large arm, coil on the small arm, and the split coil, respectively. The split coil provides the most coupling, and the coil on the large arm provides the least.

The coupling coefficients obtained by the above method decrease rapidly at higher frequencies, which is caused by parasitic capacitances shunting the receiving coil inductance. Strictly speaking, accurate inductance values can be measured only when the coil parasitic capacitance does not noticeably affect the total impedance. Therefore, our measurements are subject to greater errors at high frequency owing to increased loading from internal receiver coil parasitic capacitance. However, the capacitive susceptance at lower frequencies is small enough to be neglected, and the obtained k values in this range are valid. The coupling coefficients taken at the lower end of the curves are 0.41, 0.73 and 0.79 for the coil on the large arm, coil on the small arm and split coil, respectively.

The parasitic effects of the integrated coil can be determined by curve-fitting again the measured coil impedances using the model of Fig. 1(a). The inductance in the model should be L_2 when the wire-wound driving coil is open-circuited, and $L_{\text{leak}} = (1 - k^2)L_2$ when the coil is short-circuited. The measured impedances and the curve-fittings are presented in Fig. 5, where the coil inductances are determined as 7.6, 6.2, 3.7 and 3.0 μH, respectively, which leads to coupling coefficients of 0.429, 0.716 and 0.778, respectively. These coupling coefficients are close to those taken at low frequency in Fig. 8, thus supporting both strategies for measuring coupling coefficients.

4. Power Transfer Efficiency

With quality factors and coupling coefficients obtained in the previous section, link efficiencies are calculated using Eqs. (2) and (3), and compared with experimental results, as presented in Fig. 6. From Eqs. (2) and (3), it can be seen that link efficiency depends only on coil quality factor. Thus, driving coils of different inductances but having the same quality factors will provide the same link efficiency. This is experimentally supported by Fig. 6, which gives the measured and calculated power delivery efficiency to a 50 Ω load. In Fig. 6, the efficiencies obtained with 20-turn, 30-turn, and 40-turn driving coils produce very similar curves. It should be noted that the efficiency of power supplies and deliverable power depend on the driving coil inductance. The link efficiency drops off rapidly beyond 5 MHz, where the parasitic capacitance of the integrated coil still poses over 1 kΩ impedance while both the

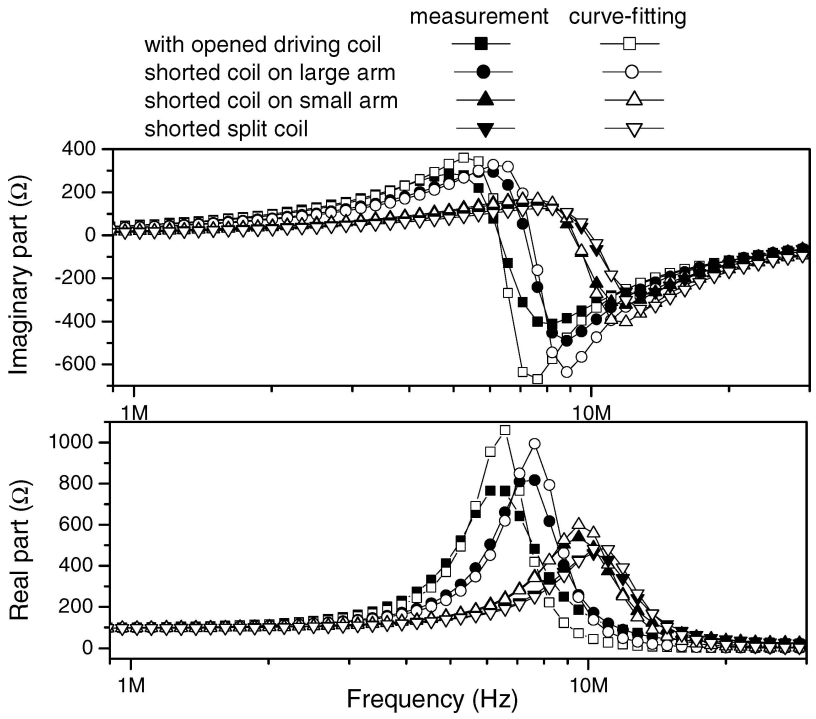

Figure 5. Curve-fitting of a 20-turn driving coil to obtain coupling coefficients.

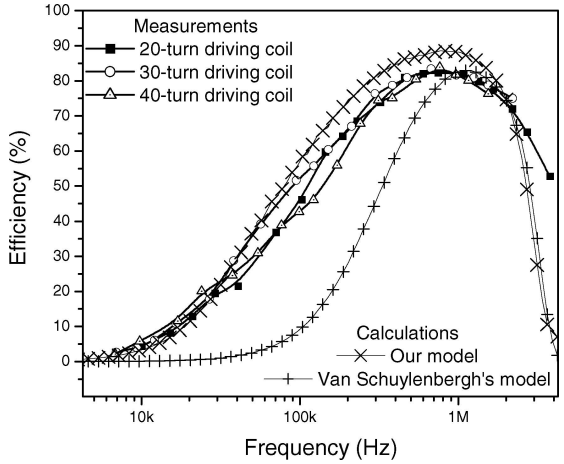

Figure 6. Comparison of link efficiency to 50 Ω load with 10 turn plated receiving coil by measurements and calculations using two models (Eqs. (2) and (3)).

load and the magnetizing inductance are no more than 100 Ω; thus it is reasonable to neglect capacitance for the operating range.

The comparison between our model and Van Schuylenbergh's is also shown in Fig. 6. Our model gives close agreement with measurements. In contrast, Van Schuylenbergh's model gives lower efficiency than measurements, especially at lower frequencies. This can be attributed to assigning all of the loss to a resistor in series with leakage inductance, which leads to excessive attenuation of power at low frequencies. With our model, the power is bypassed by the magnetizing inductance at low frequencies, since it poses little impedance.

We have also performed calculations of efficiency for links with different loads and coils, and the results exhibit good agreement with the measurements. An example is shown in Figs. 7(a) and (b), in which two types of receiving microcoils, i.e. thin film and electroplated coils, are used to deliver power to a 13 Ω load. We can see that our model provides a more accurate prediction of link efficiency than Van Schuylenbergh's. Therefore, it is reasonable to treat the energy loss mechanism of the driving coil as distributive and scale it by the coupling coefficient. Another observation is that electroplated coils indeed improve link efficiency by a great margin.

From Eq. (2), it can be derived that for a given set of coil quality factors and coupling coefficients, there

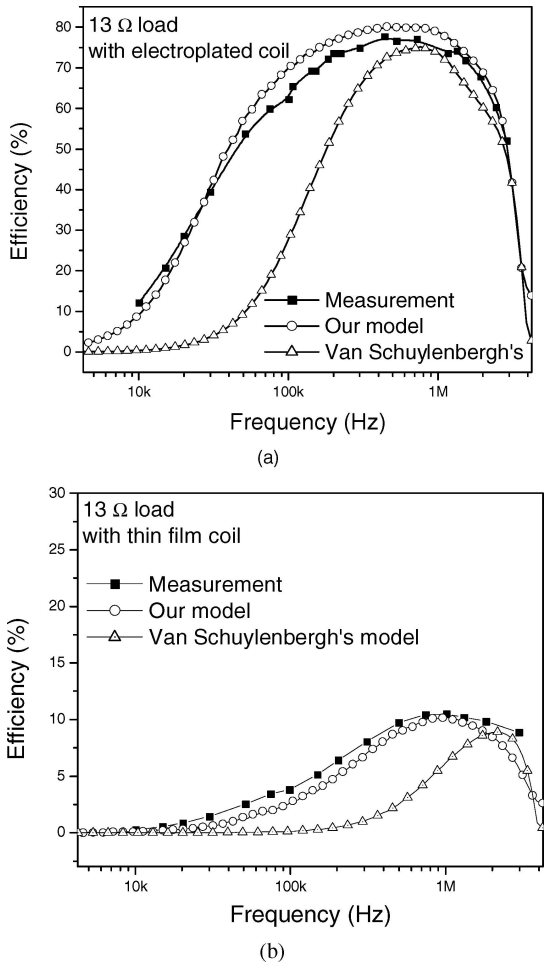

Figure 7. Measurements and calculations of link efficiency to 13 Ω load with (a) 10-turn electroplated coil and (b) 10-turn thin film coil.

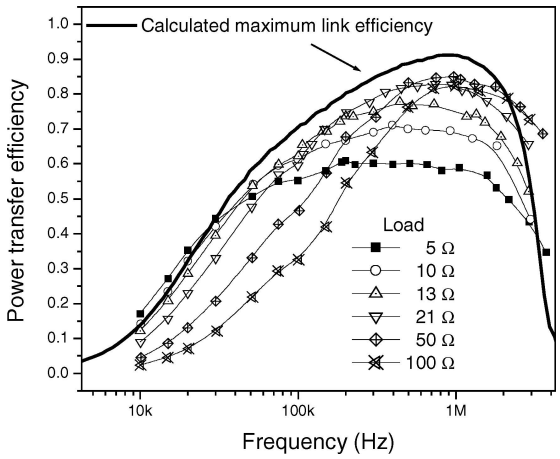

Figure 8. Calculated maximal link efficiency for the test inductive link.

is an optimal load factor, Z_O,

$$1/Z_O = \sqrt{1/Q_2^2 + (Q_1 + 1/Q_1) \times k^2/Q_2 + (Q_1 + 1/Q_1 + 2/Q_2) \times (1 - k^2)/Q_1}, \tag{4}$$

which leads to the maximal efficiency, $\eta_{\max}$:

$$\eta_{\max} = \frac{k^2(Q_1 + 1/Q_1)}{2/Z_O + 2/Q_1 + 2/Q_2 + k^2(Q_1 - 1/Q_1)}. \tag{5}$$

$\eta_{\max}$ of the test inductive link is calculated and compared with experimental efficiencies for various loads, as shown in Fig. 8. The calculated $\eta_{\max}$ is greater than, and has the same shape as, the measured values over most of the frequency range. It can be concluded that our equivalent circuit predicts the link efficiency with reasonable accuracy. Equations (4) and (5) can provide some guidance in impedance matching when trying to obtain a maximum link efficiency.

5. Summary

In this paper, an inductive link with integrated receiving coil was proposed to transfer energy onto silicon chips wirelessly, and its operation was demonstrated. Experiments and simulations were performed to characterize the coils, and determine the link efficiency. Parasitic effects associated with silicon were manifested in impedance measurements of both a wire-wound driving coil and an integrated receiving coil. Curve-fitting was used to de-embed the parasitic effects of integrated coils during the measurement of link coupling coefficient.

A modified equivalent circuit was developed in which the energy losses in the driving coil are regarded as distributed and associated with link coupling. Using measured coil parameters and coupling coefficient, calculated link efficiency shows good agreement with experiments, thus supporting the improved link equivalent circuit. The characterization methods and treatment of parasitic effects can provide a good prediction of inductive links with integrated coils.

It is experimentally verified that our model predicts the link efficiency more accurately than does the conventional model for links with two wire-wound coils. The impact of coil quality factors on link efficiency is also investigated with the model, which can provide some insights for the optimization of link efficiency under various conditions.

Acknowledgment

This work was supported by the State of Indiana and the Bayer Corporation.

References

1. N. de N. Donaldson and T.A. Perkins, *Med. & Biol. Eng. & Comput.*, **21**, 612 (1983).
2. D.C. Galbraith, M. Soma, and R.L. White, *IEEE Trans. Biomed. Eng.*, **BME-34**, 265 (1987).
3. N. de N. Donaldson, *Med. & Biol. Eng. & Comput.*, **21**, 756 (1983).
4. C.M. Zierhofer and E.S. Hochmair, *IEEE Trans. Biomed. Eng.*, **37**, 716 (1990).
5. G.B. Joung and B.H. Cho, *IEEE Trans. Power Electron.*, **13**, 1013 (1998).
6. K. Van Schuylenbergh, Optimisation of inductive powering of small biotelemetry implants, Ph.D. dissertation, Katholieke Universiteit Leuven, 1998.
7. H. Sakamoto, K. Harada, S. Washimiya, and K. Takehara, *IEEE Trans. Magn.*, **35** 3526, (1999).
8. W.J. Heetderks, *IEEE Trans. Biomed. Eng.*, **35**, 323 (1988).
9. T.H. Nishimura, T. Eguchi, A. Kubota, M. Hatori, and M. Saito, *Proc. 20th Annul Int'l Conf. IEEE Eng. in Medicine and Biol. Soc.*, **20**, 432–435 (1998).
10. J. Zhao, C.F. Foo, and K.J. Tseng, *IEEE Trans. Magn.*, **35**, 3550 (1999).
11. D. Dudenbostel, K. Krieger, C. Candler, and R. Laur, TRANSDUCERS '97, Chicago, (1997), pp. 995–998.
12. J.A. Von Arx and K. Najafi, *TRANSDUCERS '97*, Chicago, pp. 999–1002.
13. R. Puers, G. Vandevoorde, and D. De bruyker, *J. Micromech. Microeng.*, **10**, 124 (2000).
14. S. Takeuchi, N. Futai, and I. Shimoyama, MEMS 2001—14th IEEE Int'l Conf. MEMS, Interlaken, Switzerland, (2001), pp. 574–577.
15. A. DeHennis and K.D. Wise, MEMS 2002, Las Vegas, LV, (2002), pp. 252–255.
16. J.-B. Yoon, C.-H. Han, E. Yoon and C.-K. Kim, *IEEE MTT-S Int. Microwave Symp. Dig.*, 1523–1526 (June 1999).
17. J.-B. Yoon, C.-H. Han, E. Yoon and C.-K. Kim, *IEEE Int. Electron Devices Meet. Tech. Dig.*, 753–756 (1999).
18. J. Wu and G.H. Bernstein, "An inlaid electroplated copper coil for on-chip powering of MEMS devices," *J. Vac. Sci. Technol. B*, **22**, 611–618 (2004).
19. J. Wu, V. Quinn, and G.H. Bernstein, "Powering efficiency of inductive links with inlaid electroplated microcoils," *J. Micromech. Microeng.*, **14**, 576–586 (2004).
20. www.ferroxcube.com.
21. W. Bacher, W. Menz, and J. Moh, "The LIGA technique and its potential for microsystems-a survey," *IEEE Trans. Industrial Electron.*, **42**, 431–441 (1995).